Mon. Not. R. Astron. Soc. **282,** 1–12 (1996)

The tilt of the fundamental plane of elliptical galaxies – I. Exploring dynamical and structural effects

L. Ciotti,[1] B. Lanzoni[2] and A. Renzini[2,3]

[1]*Osservatorio Astronomico di Bologna, via Zamboni 33, Bologna 40126, Italy*
[2]*Dipartimento di Astronomia, Università di Bologna, via Zamboni 33, Bologna 40126, Italy*
[3]*European Southern Observatory, Garching bei München, Germany*

Accepted 1996 January 23. Received 1996 January 10; in original form 1995 June 19

ABSTRACT

In this paper we explore several structural and dynamical effects on the projected velocity dispersion as possible causes of the fundamental plane (FP) tilt of elliptical galaxies. Specifically, we determine the size of the systematic trend along the FP in the orbital radial anisotropy, in the dark matter (DM) content and distribution relative to the bright matter, and in the shape of the light profile that would be needed to produce the tilt, under the assumption of a constant stellar mass-to-light ratio. Spherical, non-rotating, two-component models are constructed, where the light profiles resemble the $R^{1/4}$ law. For the investigated models anisotropy cannot play a major role in causing the tilt, while a systematic increase in the DM content and/or concentration may formally produce it. Also a suitable variation of the shape of the light profile can produce the desired effect, and there may be some observational hints supporting this possibility. However, fine tuning is always required in order to produce the tilt, while preserving the *tightness* of the distribution of the galaxies about the FP.

Key words: galaxies: elliptical and lenticular, cD – galaxies: structure – dark matter.

1 INTRODUCTION

Elliptical galaxies do not populate uniformly the three-dimensional parameter space having as coordinates the central velocity dispersion σ_0, the effective radius R_e, and the mean effective surface brightness $I_e = L_B/2\pi R_e^2$, where L_B is the total galaxy luminosity in the blue band. They rather closely cluster around a plane (Dressler et al. 1987, hereafter D87; Djorgovski & Davis 1987; Bender, Burstein & Faber 1992, hereafter BBF; Djorgovski & Santiago 1993; and references therein) thus called the fundamental plane (FP). The existence of these 'scaling relations' is believed to be of great importance for several reasons, including the understanding of the formation and evolution of elliptical galaxies, their use as tracers of bulk motions and potentially as a cosmological probe when studying the FP relations for clusters at higher and higher redshifts.

For their sample of Virgo ellipticals BBF introduced a convenient coordinate system, where the axes are linear combinations of the observables $\log \sigma_0^2$, $\log R_e$ and $\log I_e$:

$$k_1 \equiv (\log \sigma_0^2 + \log R_e)/\sqrt{2}$$
$$k_2 \equiv (\log \sigma_0^2 + 2 \log I_e - \log R_e)/\sqrt{6} \quad (1)$$
$$k_3 \equiv (\log \sigma_0^2 - \log I_e - \log R_e)/\sqrt{3},$$

and the FP is seen edge-on when projected on the k_1–k_3 plane. The FP for Virgo ellipticals is shown in Fig. 1 and follows the relation

$$k_3 = 0.15 k_1 + 0.36, \quad (2)$$

having assumed a Virgo distance of 20.7 Mpc, and measuring σ_0, R_e and I_e respectively in km s^{-1}, kpc, and $L_{B\odot}$ pc^{-2} units (cf. BBF). The two main properties of the FP for Virgo ellipticals are the so-called *tilt*, i.e., the systematic increase of k_3 along the FP described by equation (2), and its tightness, i.e., the nearly constant and very small dispersion of k_3 at every location on the FP, with $\sigma(k_3) \simeq 0.05$.

Using the virial theorem, the ks can be related to the total galaxy mass $M = c_2 R_e \sigma_0^2$ by

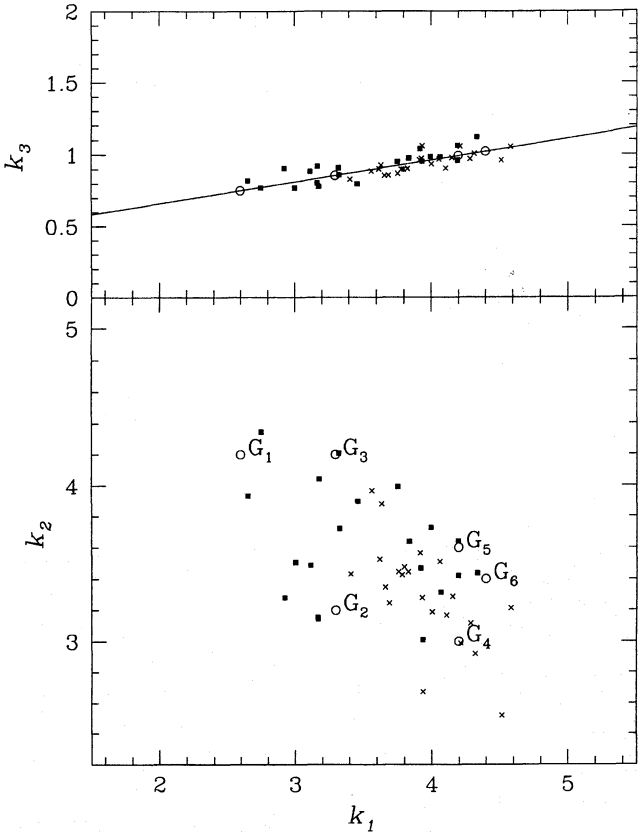

Figure 1. The distribution of Virgo (closed boxes) and Coma (crosses) ellipticals in the (k_1, k_2, k_3) space, from BBF. The upper panels shows the FP edge-on; in the lower panel the FP is seen nearly face-on. Open circles represent our reference models G_i (see Section 4.5).

$$k_1=\frac{1}{\sqrt{2}}\log\frac{M}{c_2}, \tag{3}$$

$$k_3=\frac{1}{\sqrt{3}}\log\frac{2\pi M}{L_B c_2}. \tag{4}$$

If the virial coefficient c_2 is constant for all the galaxies, the observed FP tilt as described by equation (2) implies a systematic trend in the mass-to-light ratio with galaxy luminosity: $M/L_B \propto L_B^{0.2}$ (e.g., D87). Meanwhile, the small and constant thickness of the distribution about the FP corresponds to a very small ($\lesssim$12 per cent) dispersion of M/L_B for any given luminosity. The 'smallness' of the 0.2 exponent may give the impression that the FP tilt is just a minor, not especially important, effect. However, this is a misleading impression. As galaxies in Fig. 1 span a factor $\sim$200 in luminosity, the tilt corresponds to a factor $\sim$3 increase of M/L_B along the FP, from faint to bright galaxies.

On the other hand, the virial coefficient c_2 depends on the mass, light and velocity dispersion distributions within the galaxy, and is constant only insofar as all such distributions are homologous. It can be obtained by solving the Jeans equations, for any reasonable assumption concerning the distribution of the bright and DM components, and the orbital anisotropy, with the additional constraint that the star density distribution will reproduce the observed galaxy surface brightness profile.

Considering only the stellar component (i.e., the fraction of the total mass whose density follows the light distribution), its mass M_* can be expressed as

$$M_*=c_2^* R_e \sigma_0^2, \tag{5}$$

where $c_2^*=c_2$ in the case of a galaxy that is devoid of dark matter ($M_*=M$), while, and in general,

$$\frac{M_*}{c^*}=\frac{M}{c_2}. \tag{6}$$

Substituting (6) into (3) and (4) we see that the origin of the FP tilt can be sought in two *orthogonal* directions: either the tilt may arise from a *stellar population* effect ($\Upsilon_*\equiv M_*/L_B \propto L_B^{0.2}$ while $c_2^*=$constant) or from a *structural/dynamical* effect ($c_2^* \propto L_B^{-0.2}$ while $\Upsilon_*=$constant). In the former case, the tilt would result from a trend in some combination of typical stellar metallicity, age and initial mass function (IMF). A priori this appears to be a quite viable option: after all, a systematic trend in colour and line strengths is known to exist with galaxy luminosity (hence with k_1), which is usually ascribed to a trend in the mean metallicity with the depth of the galactic potential well. However, the metallicity effect has been estimated to be marginal (D87; Djorgovski & Santiago 1993), and indeed existing population synthesis models appear to fail to reproduce but a small fraction of the tilt, unless special conditions are verified (Renzini 1995). On the other hand, a drastic variation of the IMF along the FP is required to produce the tilt, with M/brown dwarfs turning from being a minor constituent to one that dominates the baryonic mass of ellipticals, yet with a very small dispersion of the IMF at any location on the FP (Renzini & Ciotti 1993, hereafter RC). A search for the origin of the FP tilt in this direction will be further pursued in a separate paper (Maraston, Renzini & Ritossa, in preparation).

In this paper we concentrate instead on the second option, assuming a constant stellar mass-to-light ratio Υ_*, and exploring under which conditions structural/dynamical effects may cause the tilt in k_3 via a systematic decrease of c_2^*. Although a contribution to the tilt may derive also from a trend in the rotational support (decreasing from faint to bright ellipticals; e.g., Davies et al. 1983), we concentrate here on the effects of systematic trends along the FP in (1) the degree of radial anisotropy of the velocity dispersion tensor, (2) the DM fraction and/or distribution within the galaxies, and (3) the density profile of the bright component. Concerning the dark matter, a preliminary exploration led to conclude that the central regions of ellipticals should turn from being baryon dominated to being DM dominated with increasing L_B, again with fine tuning required to account for the tilt and yet preserve the observed small and constant thickness of the FP (RC). A break in the structural homology as a possible origin of the tilt has been suggested by Djorgovski (1995) and Hjorth & Madsen (1995).

In Section 2 we briefly describe the dynamical models that we have used for exploring points (1) and (2), and derive an analytical approximation for the virial coefficient c_2^*. In Section 3 we investigate anisotropy as a possible cause of the FP tilt, while in Section 4 we explore the effects of the

amount and distribution of DM, in every case having assumed a fixed shape for the light profiles of all the galaxies. Projected velocity dispersion profiles are computed for models that succeed in producing the k_3 tilt. In conjunction with available observations these profiles are then used to reject some classes of models and to suggest a future observational test for those that still survive. Having completed the analysis of the *dynamical* options for the origin of the tilt, in Section 5 we pass to investigate the *morphological* option. This is accomplished by assuming isotropic models without DM, whose surface brightness distribution is described by $R^{1/m}$ profiles, thus ascribing to a systematic variation of m the origin of the tilt. Finally, in Section 6 we discuss and summarize the results.

2 THE MODEL GALAXIES

We make use of four classes of two-component, spherical galaxy models, totally velocity-dispersion supported. We indicate with r the spatial radial coordinate and with R the projected one.

2.1 Bright and dark matter distributions

As is well known, the empirical $R^{1/4}$ law (de Vaucouleurs 1948) suitably fits the observed surface brightness profiles of many elliptical galaxies, but its deprojection cannot be expressed in terms of elementary functions. For this reason we describe the stellar component by two density distributions which give a good approximation to the $R^{1/4}$ law when projected, and at the same time permit several fully analytical manipulations. We consider the Hernquist (1990) density law,

$$\rho_*(r)=\frac{M_*}{2\pi}\,\frac{r_*}{r(r_*+r)^3}, \tag{7}$$

for which the effective radius $R_e\simeq 1.82r_*$, and the Jaffe (1983) density law,

$$\rho_*(r)=\frac{M_*}{4\pi}\,\frac{r_*}{r^2(r_*+r)^2}, \tag{8}$$

for which $R_e\simeq 0.76r_*$.

The density law appropriate for dark haloes in elliptical galaxies is yet to be determined. The same kind of density profile – although with different masses and scalelengths, i.e., with M_D and r_D replacing M_* and r_*, respectively – may apply in the description of the luminous and dark matter distributions in a scenario in which both are collisionless and have undergone similar dynamical processes during galaxy formation, yet have started from different initial conditions (e.g., Bertin, Saglia & Stiavelli 1992, hereafter BSS). On the other hand, the distributions of the dark and bright matter may have different shapes to the extent that the baryonic component has dissipated, thus sinking deeper into the potential well.

In the first option, DM haloes present a central cusp (e.g., Dubinski & Carlberg 1991; BSS; Kochanek 1993, 1994), and in this mood we investigate HH models, where both the luminous and the dark components are described by a Hernquist distribution, and JJ models where both follow a Jaffe profile. In the mood of dissipational collapse, we investigate two other classes of models where the dark halo density flattens at small radii, while the stellar distribution peaks towards the centre. In the first class, which we call HP models, the Hernquist luminous component is embedded in a Plummer (1911) dark halo:

$$\rho_D(r)=\frac{3M_D}{4\pi}\,\frac{r_D^2}{(r_D^2+r^2)^{5/2}}; \tag{9}$$

in the other class (JQ models), the stellar component is described by the Jaffe formula and the dark halo by a truncated quasi-isothermal distribution:

$$\rho_D(r)=\begin{cases}\rho_{D0}r_D^2(r_D^2+r^2)^{-1} & \text{for } r\le r_t;\\ 0 & \text{for } r>r_t.\end{cases} \tag{10}$$

2.2 The dynamical models

In order to compare our models with the dynamical properties of the observed galaxies, we need their spatial and projected velocity dispersion profiles. These are obtained by solving the associated Jeans equation (see, e.g., Binney & Tremaine 1987, hereafter BT):

$$\frac{\mathrm{d}\rho_*(r)\sigma_r^2(r)}{\mathrm{d}r}+\frac{2\alpha(r)\rho_*(r)\sigma_r^2(r)}{r}=-\frac{GM(r)}{r^2}\rho_*(r), \tag{11}$$

with the boundary condition $\rho_*(r)\sigma_r^2(r)\to 0$ for $r\to\infty$, where $M(r)$ is the mass within r. We use for $\alpha(r)$ the Osipkov–Merritt formula,

$$\alpha(r)\equiv 1-\frac{\sigma_\theta^2(r)}{\sigma_r^2(r)}=\frac{r^2}{r^2+r_a^2} \tag{12}$$

(Osipkov 1979; Merritt 1985a,b), so that the velocity dispersion tensor is nearly isotropic inside r_a and radially anisotropic outside, consistent with N-body simulations (see, e.g., van Albada 1982). Analytical expressions for the radial velocity dispersion profiles of HH, HP and JJ models are given in the Appendix. Their projection is then obtained by (e.g., BT, p. 208) using

$$\sigma_P^2(R)=\frac{2}{\Sigma_*(R)}\int_R^\infty\left[1-\alpha(r)\frac{R^2}{r^2}\right]\frac{\rho_*(r)\sigma_r^2(r)r}{\sqrt{r^2-R^2}}\,\mathrm{d}r, \tag{13}$$

where $\Sigma_*(R)=\Upsilon_* I(R)$ is the surface stellar mass density. The solution of (11) then provides the projected velocity dispersion profile, via equation (13).

Having fixed Υ_* over all the FPs, a galaxy model is therefore specified by five more parameters, namely M_*, r_* (or R_e), M_D, r_D and the anisotropy radius r_a. In the following, we replace M_D and r_D with the dimensionless ratios $\mathscr{R}=M_D/M_*$ and $\beta=r_D/r_*$.

The observed σ_0 entering into the definitions of the ks in (1) does not correspond to $\sigma_P(0)$, but rather to the average over the aperture used for the spectrographic observations. That used by D87 for constructing the ks of the Virgo galaxies in Fig. 1 was normalized to a 4×4 arcsec^2 aperture at Coma distance. The average of $\sigma_P(R)$ over such a rectangular aperture being very similar to that over a circular

aperture of 2.2 arcsec radius, we simulate σ_0 by

$$\sigma^2_{ap}(R_{ap}) = \frac{2\pi}{M^*_P(R_{ap})} \int_0^{R_{ap}} \Sigma_*(R)\,\sigma^2_P(R)\,R\,dR, \qquad (14)$$

where $M^*_P(R_{ap})$ is the projected stellar mass inside R_{ap}. We therefore mimic the actual observations if considering $\sigma_{ap} \equiv \sigma_0$, and we correspondingly obtain the virial coefficient c^*_2 from equation (5). The ks are then obtained from (3), (4) and (6).

Instead of a fixed angular aperture (as used by D87), when calculating σ_{ap} we have, for simplicity, adopted a fixed *linear* aperture $R_{ap} = 0.02R_e$ for all our models. As discussed in Section 4.3, such a choice has a negligible effect on our results.

2.3 An analytical approximation

The described procedure to determine c^*_2 and the ks for a specified set of parameters r_a, $\mathscr{R}$ and β was performed numerically solving (11)–(14) for a three-dimensional grid: $(r_a, \mathscr{R}, \beta) \in [(r_a)_{min}, \infty[\times [0, 10] \times [0.1, 40]$, where $(r_a)_{min}$ is the lower acceptable limit for the anisotropy radius as discussed in Section 3. We express the resulting c^*_2 in the form

$$c^*_2 = \frac{A(R_{ap})}{\Theta(r_a, \mathscr{R}, \beta)}, \qquad (15)$$

where A is the virial coefficient in the absence of both DM and anisotropy, and Θ represents the correcting factor when such ingredients are included. In units of $M_\odot\ s^{-2}\ kpc^{-2}\ km^{-2}$ the value of $A(0.02R_e)$ is 1.74×10^6 and 6.49×10^5 for a Hernquist and a Jaffe stellar distribution, respectively. A good fit (within 5 per cent) for the numerical values of Θ for HH, HP and JJ models is given by

$$\Theta(r_a, \mathscr{R}, \beta) = \left[1 + \frac{B}{(r_a/R_e)^b}\right] \times \left\{1 + \mathscr{R}\,\frac{C}{\beta^c(\beta + D)^d}\left[1 + \frac{E(\beta)}{[(r_a/R_e) + F(\beta)]^{f(\beta)}}\right]\right\}, \qquad (16)$$

with all the coefficients and exponents being reported in Tables 1 and 2.

The adopted form of the function Θ retains the main physical constraints of the problem. Indeed, $\Theta \to 1$ for $r_a \to \infty$, and $\mathscr{R} \to 0$ or $\beta \to \infty$. The linear dependence on $\mathscr{R}$ derives directly from (11). We did not attempt an analytic fit for the JQ models.

Table 1. Numerical values of the fitting β-independent parameters in equation (16).

	B	b	C	c	D	d
HH	0.076	1.47	1.70	0.96	0.70	0.980
HP	0.076	1.47	1.58	1.21	0.95	1.695
JJ	0.009	1.36	1.06	0.48	0.05	0.515

2.4 Constraining models to the fundamental plane

In order to constrain the models to lie on the FP , the value of Θ at each k_1 is determined using (6), (4) and (15):

$$\Theta = \frac{A}{2\pi\Upsilon_*}\,10^{0.26k_1 + 0.62}, \qquad (17)$$

and therefore the required trend in either r_a, $\mathscr{R}$ or β as a function of k_1 is derived. The stellar mass-to-light ratio Υ_* is obtained from (17) with $k_1 = 2.6$ and $\Theta = 1$, which corresponds to assuming the faintest galaxies to be isotropic and devoid of DM. For Hernquist models we find $\Upsilon_* = 5.5$, while for Jaffe ones we have $\Upsilon_* = 2.06$.

3 MAKING THE FP TILT WITH A TREND IN THE ANISOTROPY

In this section we ascribe the entire tilt of the FP to a trend with L_B in the anisotropy degree of the galaxies (i.e., in r_a), assuming no DM. The values of the anisotropy radius at each location on the k_1 axis are determined by solving (17) and then (16) for r_a, with $\mathscr{R} = 0$. The results are shown in Fig. 2 for a Hernquist and a Jaffe stellar distribution. The

Table 2. Some numerical values of the fitting β-dependent parameters in equation (16) for HH (columns 2–4), HP (columns 5–7) and JJ models (columns 8–9; in this case, $f(\beta) = 12.5$ for every value of β).

β	$E(\beta)$	$F(\beta)$	$f(\beta)$	$E(\beta)$	$F(\beta)$	$f(\beta)$	$E(\beta)$	$F(\beta)$
0.2	-1.00	1.138	4.40	-1.00	1.278	4.10	-1.00	1.143
0.5	-1.00	1.308	4.70	-1.00	1.191	6.00	-1.00	1.235
1.0	1.00	21.67	4.50	1.00	0.946	3.55	-1.00	2.002
1.5	1.00	1.437	4.60	2.82	1.115	3.73	1.00	1.312
2.0	1.00	1.278	4.40	3.69	1.122	3.58	1.00	1.261
2.5	1.00	1.229	3.90	3.90	1.086	3.39	1.00	1.238
3.0	1.00	1.176	3.75	4.25	1.071	3.28	1.00	1.223
3.5	1.00	1.142	3.55	4.44	1.051	3.16	1.00	1.214
4.0	1.00	1.111	3.45	4.55	1.028	3.07	1.00	1.207
4.5	1.00	1.086	3.35	4.57	1.004	2.97	1.00	1.202
5.0	1.00	1.063	3.30	4.86	1.000	2.92	1.00	1.197
5.5	1.00	1.044	3.25	5.08	0.996	2.88	1.00	1.194
6.0	1.00	1.028	3.20	4.95	0.968	2.79	1.00	1.191

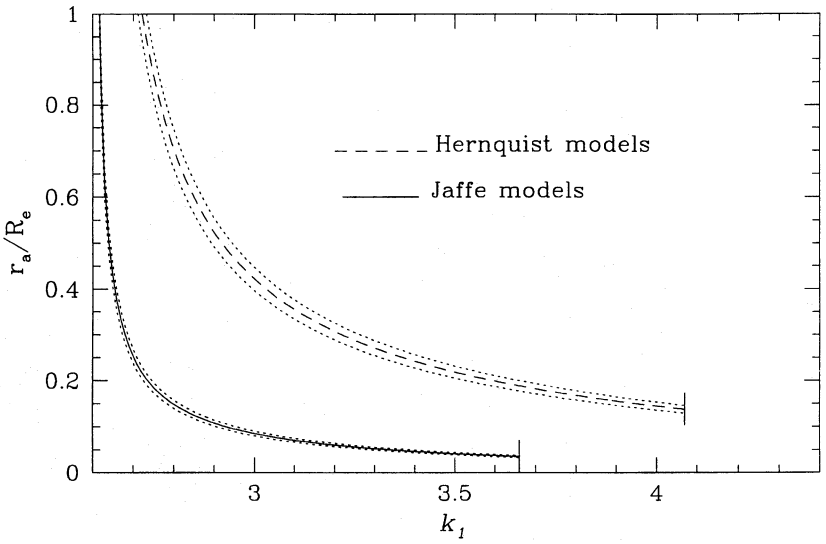

Figure 2. The trend of the anisotropy radius along the FP required to produce its tilt, in Hernquist and Jaffe models. The curves are truncated at the radius below which the models become dynamically inconsistent. The band within dotted lines marks the boundaries within which r_a can vary at each location on the k_1-axis in accordance with the observed FP tightness.

curves are truncated because of the limits imposed by dynamical consistency: above a certain luminosity, in models constrained to the FP, the phase-space distribution function runs into negative values. The limits can easily be established in the frame of the Osipkov–Merritt relation for $\alpha(r)$, without having to know the distribution function of the system (Ciotti & Pellegrini 1992). We find that $r_a \gtrsim 0.25 r_* \simeq 0.138 R_e$ for the Hernquist models and $r_a \gtrsim 0.05 r_* \simeq 0.036 R_e$ for the Jaffe ones.

Thus, we conclude that anisotropy alone cannot be at the origin of the tilt, since the extreme values of r_a that would be required correspond to dynamically inconsistent models. Note that another argument militates against radial anisotropy as the cause of the FP tilt: the requirement of radial orbit stability is much more stringent than the simple dynamical consistency, and $(r_a)_{min}$ increases again.

4 MAKING THE FP TILT WITH A TREND IN EITHER THE DARK MATTER FRACTION OR DISTRIBUTION

Following the negative results of the previous section, we assume global isotropy and move to explore DM as being potentially responsible for the tilt of the FP. We first ascribe all the tilt to a trend in the dark-to-bright mass ratio $\mathscr{R}$ at constant β, and then to a trend in the relative dark and bright distributions β at constant $\mathscr{R}$.

4.1 Varying the amount of DM

We set $r_a = \infty$, β = constant, and for $2.6 \leq k_1 \leq 4.4$ we determine the value of $\mathscr{R}$ that is required to place the models on the FP. Then $\mathscr{R}$ is obtained from equations (16) and (17) for HH, HP and JJ models, and numerically for JQ models. Obviously, the larger the value of β, the larger the variations of $\mathscr{R}$ that are required to produce the tilt. Values of $\beta \lesssim 1$ may have a mere academic interest, although some evidence seems to exist in support of a dark halo that is more centrally concentrated than the bright component (Saglia, Bertin & Stiavelli 1992, hereafter SBS). By analogy with spiral galaxies, haloes are generally considered diffuse ($\beta > 1$), although in some cases with significant amounts of DM inside the half-light radius (SBS).

Concerning HH and HP models, for $\beta \simeq 5$ exceedingly large values of $\mathscr{R}$ are required to produce the FP tilt ($\mathscr{R} \simeq 30$–175), thus we conclude that an increasing DM content from faint to bright galaxies may be at the origin of the observed tilt, provided that $\beta < 5$.

The same problem affects all the JQ models that we have considered, for all values of β and r_t.

As regards JJ models, $\mathscr{R}$ never becomes larger than 10 (for instance $\mathscr{R} \simeq 9.5$ at the bright end of the FP for $\beta = 5$), thus every value of this parameter is acceptable, for every explored value of β. Fig. 3 (upper panels) shows the results for HH and JJ models, in the cases $\beta = 1$, 2 and 5.

4.2 Varying the relative concentration of dark and bright matter

We now assume the dark-to-bright matter ratio $\mathscr{R}$ to be constant among the reference sample of elliptical galaxies, and require that the relative concentration of the two components (β) produces the observed tilt in k_3. Thus, the values of β along the FP are derived for $r_a \to \infty$ and $\mathscr{R} = 1$, 5 and 9. For every class of models we find that if $\mathscr{R} = 1$, the DM in the brightest galaxies should be more centrally concentrated than the luminous component ($\beta < 1$). Values of $\beta > 1$ at every location on the FP always require a prevalence of DM with respect to bright matter ($\mathscr{R} > 1$), apart from JQ models, which are again completely unsatisfactory, their values of β being unrealistically small for every choice of $\mathscr{R}$ (we therefore reject this class of models). Fig. 3 (lower panels) shows the trend of β along the FP for HH and JJ models.

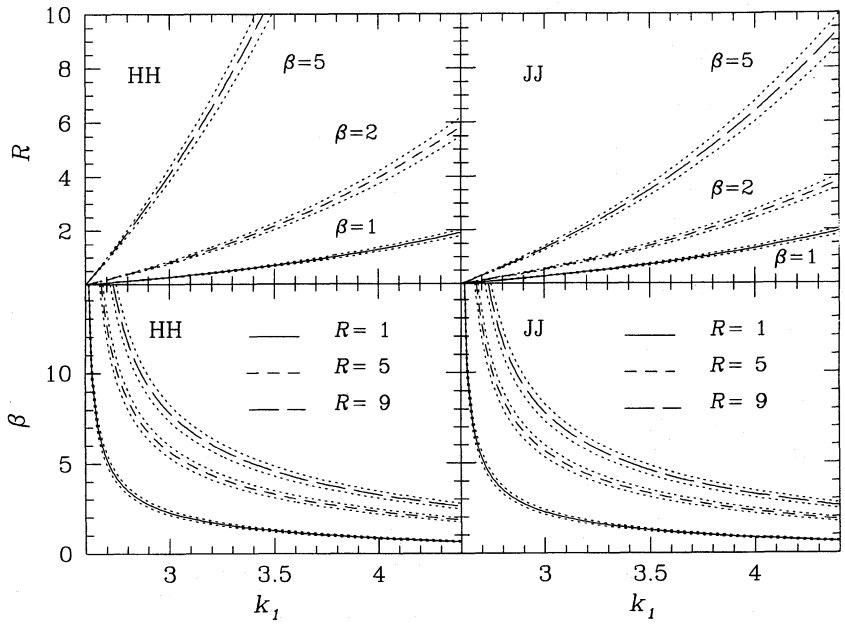

Figure 3. The trend along the FP of the DM content (upper panels) at constant β and that of the DM concentration (lower panels) at constant $\mathscr{R}$, required to produce the tilt, in HH and JJ models. The band within dotted lines marks the boundaries within which $\mathscr{R}$ and β can vary at each location on the k_1-axis in accordance with the observed FP tightness.

4.3 Aperture effect

Having used a fixed angular aperture, D87 have sampled a larger fraction of the total light (or effective radius) in fainter/smaller galaxies compared to brighter/larger galaxies. In fact, the effective radii of the galaxies in Fig. 1 range from $\sim$0.5 up to $\sim$10 kpc, and therefore a circular aperture of 2.2 arcsec (i.e., $\sim$220-pc radius at the adopted Virgo distance) corresponds to a circular region of $\sim 0.44R_e$ radius at the faint end of the FP, and of only $\sim 0.02R_e$ radius in galaxies at the bright end. When calculating σ_{ap}, we have instead adopted a fixed linear aperture of $R_{ap}=0.02R_e$ radius, thus correctly simulating only the observed σ_0 of the brightest galaxies and underestimating the fraction of effective radius sampled in the spectroscopic observations of fainter galaxies. Thus the derived c_2^*, and the corresponding values of the parameter responsible for the FP tilt, are biased by such a choice. Indeed, $\mathscr{R}(\beta)$ is set equal to 0 (∞) at the faint end of the FP, and therefore also the lower limit of the driving parameter is not affected by the *aperture bias*. Thus, the derived variation range of the parameters is correct, the main effects concerning the intermediate values of $\mathscr{R}$ and β, and the curves in Fig. 3 may be modified in their shape only in the range between the start and end points. On the other hand, a constant aperture radius for all the models has permitted us to express the correcting factor Θ in a simple analytical form.

4.4 Constraints from the tightness of the FP

The narrow and nearly constant thickness of the distribution of the galaxies about the FP (in the k_3 direction) corresponds to a very small ($\lesssim$12 per cent) dispersion in the ratio of M/L_B to the corresponding virial coefficient. If M/L_B ratios and virial coefficients are not finely anticorrelated, this indeed implies a very small dispersion, separately for both quantities, at any location on the FP. In the frame of our basic assumption ($\Upsilon_* =$ constant), this sets a very severe restriction on c_2^*, hence on Θ:

$$\frac{\delta\Theta}{\Theta} \lesssim 0.12, \tag{18}$$

which translates into strong constraints on the range that each parameter can span at any location on the FP. These can be easily derived analytically from equation (16), for the three classes of models. For HH and JJ, the dotted lines in Fig. 3 represent the band within which galaxy-to-galaxy variations of the corresponding parameter are allowed, and yet are consistent with the restrictions imposed by the tightness of the FP, i.e., with inequality (18).

It is evident from these figures that, whatever the structural parameter that is responsible for the tilt of the FP, and whatever the assumed mass distribution, dramatic fine tuning is required to produce the tilt, and yet preserve the tightness of the FP (RC).

Note that also $\delta r_a/r_a$ should be very small at each location on the FP (see the dotted band in Fig. 2), thus once more arguing against such an origin of the tilt.

4.5 Constraints from the velocity dispersion profiles

In the assumption of global isotropy, the observation of the radial trend of $\sigma_P(R)$ may hopefully give insight on the DM content and distribution within the galaxies (e.g., SBS; Bertin et al. 1994; Carollo & Danziger 1994a,b; Carollo et al. 1995, and references therein). A comparison between theoretical and observed σ_P profiles may therefore allow us to check the reliability of our models and test whether or not the DM is responsible for the FP tilt (cf. RC). In this frame, we have computed the σ_P profiles of six reference models for every class, and for all the explored combinations of $\mathscr{R}$ and

β. We have chosen six FP locations (k_1, k_2) within the portion of the FP actually occupied by Virgo ellipticals (see Fig. 1, open circles):

$G_1=(2.6, 4.2)$ $G_2=(3.3, 3.2)$ $G_3=(3.3, 4.2)$

$G_4=(4.2, 3.0)$ $G_5=(4.2, 3.6)$ $G_6=(4.4, 3.4)$,

where $G=G(k_1, k_2)$. G_1 corresponds to the faintest model, G_6 to the brightest one, while models in the pairs G_2, G_3 and G_4, G_5 only differ for the effective radius (and then the surface brightness). Their luminosities and effective radii are determined by inverting (1), (2) and (15),

$$L_B = 2\pi\ 10^{1.15k_1 - 0.62}$$

$$R_e = 10^{1.07k_1 - 0.41k_2 - 0.21},$$

and are reported in Tables 3 and 4. For HH, HP and JJ models, some representative profiles are shown in Fig. 4 (namely, those corresponding to the cases where $\mathcal{R}$ varies at constant $\beta=2$, and β varies at constant $\mathcal{R}=5$). The values of $\mathcal{R}$ and β in each model G_i are reported in Tables 3 and 4.

HH models, especially those at the bright end of the FP, are characterized by a sizeable central depression in their σ_P, while the observed profiles typically decrease monotonically with radius, at least for $R \gtrsim 0.2R_e$ (Carollo & Danziger 1994a,b). Therefore the models which better agree with observations are those in which the off-centre maximum of σ_P lies inside this radius, i.e., those where $\mathcal{R}$ varies at $\beta \lesssim 2$, and where β varies at $\mathcal{R} \lesssim 5$. In the case of HP models, the σ_P profiles always present a prominent off-centre maximum, and they have to be rejected. On the contrary, the velocity dispersion profiles of JJ models are monotonically decreasing with radius for every explored value of $\mathcal{R}$ and β, and therefore are consistent with observations. To permit a more quantitative comparison between

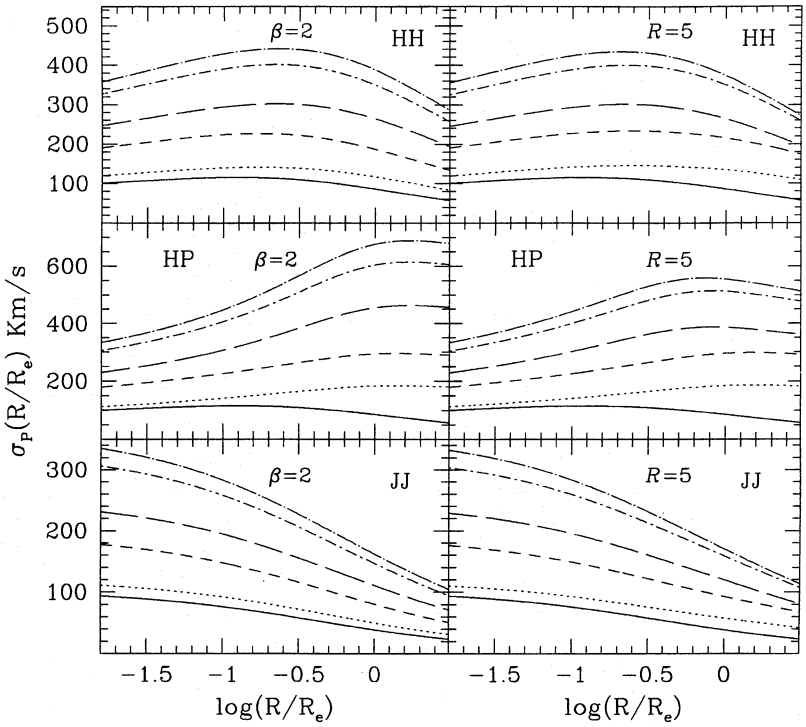

Figure 4. Projected velocity dispersion profiles of HH, HP and JJ isotropic models with variable $\mathcal{R}$ and constant $\beta=2$ (left panels), and with variable β and constant $\mathcal{R}=5$ (right panels). The solid line corresponds to the faintest reference model (G_1), while dotted, dashed, long-dashed, dot–dashed, and dot–long-dashed lines correspond to models $G_2,\ldots,G_6$, respectively.

Table 3. HH and HP models: values of L_B and R_e for the six reference models G_i, and the corresponding values of $\mathcal{R}$ for constant $\beta=2$, and of β for constant $\mathcal{R}=5$ (columns 4–5 for HH models and 6–7 for HP).

	L_B $[10^{10}M_\odot]$	R_e [kpc]	$\mathcal{R}$ $(\beta=2)$	β $(\mathcal{R}=5)$	$\mathcal{R}$ $(\beta=2)$	β $(\mathcal{R}=5)$
G_1	0.15	0.49	0.0	∞	0.0	∞
G_2	0.96	3.41	1.57	3.94	4.75	2.04
G_3	"	1.33	"	"	"	"
G_4	10.55	14.91	4.85	2.06	14.66	1.25
G_5	"	8.48	"	"	"	"
G_5	17.95	13.62	5.85	1.84	17.68	1.14

Table 4. JJ models: values of L_B and R_e for the six reference models G_i, and the corresponding values of $\mathcal{R}$ for constant $\beta=2$, and of β for $\mathcal{R}=5$.

	L_B [$10^{10}\ M_\odot$]	R_e [Kpc]	$\mathcal{R}$ ($\beta=2$)	β ($\mathcal{R}=5$)
G_1	0.15	0.49	0.0	∞
G_2	0.96	3.41	1.02	10.7
G_3	"	1.33	"	"
G_4	10.55	14.91	3.16	3.31
G_5	"	8.48	"	"
G_5	17.95	13.62	3.81	2.72

Table 5. Per cent slope of projected velocity dispersion profile as defined in equation (19) for JJ models.

	G_1	G_2, G_3	G_4, G_5	G_6
$\mathcal{R}(\beta=0.2)$	57%	62%	67%	68%
$\mathcal{R}(\beta=0.5)$	57%	59%	61%	62%
$\mathcal{R}(\beta=1.0)$	57%	57%	57%	57%
$\mathcal{R}(\beta=2.0)$	57%	53%	50%	50%
$\mathcal{R}(\beta=5.0)$	57%	48%	43%	42%
$\beta(\mathcal{R}=1.0)$	57%	53%	61%	63%
$\beta(\mathcal{R}=5.0)$	57%	46%	46%	47%
$\beta(\mathcal{R}=9.0)$	57%	45%	42%	42%

the models and the observed velocity dispersion profiles, in the JJ case we define a slope of $\sigma_P(R)$ as

$$\Delta\sigma(R)=1-\frac{\sigma_P(R)}{\sigma_P(0)}, \tag{19}$$

where $\sigma_P(0)$ is the maximum (i.e., the central) value of the projected velocity dispersion. Table 5 gives the values of $\Delta\sigma$ for the six G_i models and for $R=2R_e$, a typical value for the outermost determinations of $\sigma_P(R)$ (Bertin et al. 1994). Using these values we can recognize characteristic trends in the slope inside each scenario.

In fact, in the assumption that $\mathcal{R}$ varies from faint to bright galaxies at β constant less than unity, $\Delta\sigma(2R_e)$ monotonically increases along the FP, i.e., the σ_P profiles systematically become steeper as galaxy luminosity increases. If $\beta=1$, instead, the slope of the σ_P profiles is the same for every model, no matter what is the luminosity, while if $\beta>1$, it systematically decreases along the FP. This can be easily understood as the velocity dispersion profiles reflect the potential well of the systems. Thus, if $\beta<1$ an increasing $\mathcal{R}$ along the FP corresponds to an increase of DM content in the inner regions of galaxies, while if $\beta>1$ external regions are involved. In the first case velocity dispersion increases at small radii and then σ_P profiles steepen, while in the second case effects concern external parts of profiles and thus they flatten along the FP. If $\beta=1$ instead, the potential well only deepens, but does not become narrower or wider and velocity dispersion profiles do not vary their slope.

In the frame of the second scenario ($\mathcal{R}$ constant and β decreasing along the FP) velocity dispersion profiles initially flatten and then steepen as luminosity of the galaxies increases. From previous assumptions G_1 is an isotropic and DM lacking galaxy, so the required condition $\beta(G_2)<\beta(G_1)$ is equivalent to having added a DM component in the external regions of the G_2 model. Consequently, the external velocity dispersion increases and $\sigma_P(R)$ flattens. Moving towards the bright end of the FP, β decreases, the DM is more and more pushed towards central regions and there is a critical value β_{crit} when DM starts affecting the central parts of the $\sigma_P(R)$ profiles, rather than their external wings. Thus $\sigma_P(R)$ steepens for $\beta<\beta_{crit}$.

In conclusion, observations may, in principle, be used to check whether the FP tilt can be ascribed to a trend of $\mathcal{R}$ at $\beta=$constant, or if it is caused by a variation of β at $\mathcal{R}=$constant, or whether a dynamical origin has to be rejected. In the first case it is also possible to determine whether DM in galaxies is more or less concentrated than the bright component, or if they are distributed in the same way.

5 MAKING THE FP TILT WITH A TREND IN THE SURFACE BRIGHTNESS PROFILE

Systematic deviations of the light distributions of ellipticals from the standard $R^{1/4}$ profile may also possibly cause the FP tilt (Djorgovski 1995; Hjorth & Madsen 1995). In this section we explore such a possibility through a class of models in which the log of the surface brightness is proportional to $R^{1/m}$ and m is allowed to vary with the luminosities of the galaxies. We assume global isotropy and no DM, thus c^*_2 depends only on the stellar density distribution, and we determine which variation of m along the FP is required to generate the tilt.

5.1 The models

The surface brightness distribution of $R^{1/m}$ models is described by the generalized de Vaucouleurs law (Sersic 1968)

$$I(R)=I_0\exp[-b(m)(R/R_e)^{1/m}], \tag{20}$$

where $b(m)\simeq 2m-0.324$ for $0.5\le m\le 10$ (Ciotti 1991). The dynamical properties of this class of models are determined by solving equations (11)–(14) with $\alpha(r)=0$. In this case the virial coefficient c^*_2 depends on the aperture radius R_{ap} in a non-trivial way. Thus, to correctly simulate real observations, equation (14) is solved by averaging $\sigma_P(R)$ over a fixed angular aperture of 1.6 arcsec radius, i.e., a suitably varying R_{ap}/R_e with galaxy luminosity.

5.2 The tilt and the tightness

Assuming faintest galaxies to be $R^{1/4}$ systems, by analogy with Section 2, we set

$$c^*_2=\frac{A_4(R_{ap})}{\Theta(m)}, \tag{21}$$

where A_4 is the virial coefficient for $m=4$ and Θ represents the correcting factor when $m\neq 4$. In order to produce the tilt, this has to increase from 1 to ~ 3 along the FP. The values of m that force the six reference models G_i to lie on the FP have been correspondingly determined: the result is that m has to increase from 4 (G_1) up to ~ 10 (G_6) along the

k_1, as shown in Fig. 5 (upper panel). The figure also shows the band within which m can vary for fixed luminosity consistently with the tightness of the FP. Once again, a fine tuning of the driving parameter is required to fit the observations: a very small ($\lesssim$10 per cent) scatter of m at any location on the FP should be associated with a large variation of it with luminosities of the galaxies. If one assumes instead that $m=2$ for the faintest galaxies (model G_1), the required variation is even larger, about a factor of 4, up to $\sim$8 for the model G_6, and the permitted variation of it at each FP location remains very small (Fig. 5, lower panel).

5.3 Comparison with observations

It actually turns out that the surface brightness distribution of ellipticals is well described by $R^{1/m}$ profiles with variable m, any model with $3<m<10$ being hardly distinguishable from the $R^{1/4}$ law in the radial range usually covered by observations (Makino, Akiyama & Sugimoto 1990). However, a systematic trend of m with galaxy luminosity has recently been reported (Caon, Capaccioli & D'Onofrio 1993, hereafter CCD), with m increasing from $\sim$1 up to $\sim$15, thus spanning a much wider range than required to produce the tilt. Indeed, if one is restricted to the Virgo galaxies in common with BBF, excluding three (NGC 4406, 4552 and 4621), m ranges between $\sim$2 and $\sim$8, in good agreement with the required increase of m from faint to bright galaxies. The apparently large dispersion inferred by observations is worrisome, with m varying by a factor $\sim$3 at any given luminosity (see Fig. 6), at variance with the observed FP tightness.

A conclusion that is implicit in the BBF study seems to be at variance with m as a possible cause of the FP tilt. As the ratio between the tidal radius r_t and the core radius r_c is about 100–300 for giant ellipticals, when described by King (1966) models, one may suppose that the faintest galaxies have $r_t/r_c=100$ and the brightest ones $r_t/r_c=300$, thus showing a trend in the bright matter distribution along the FP.

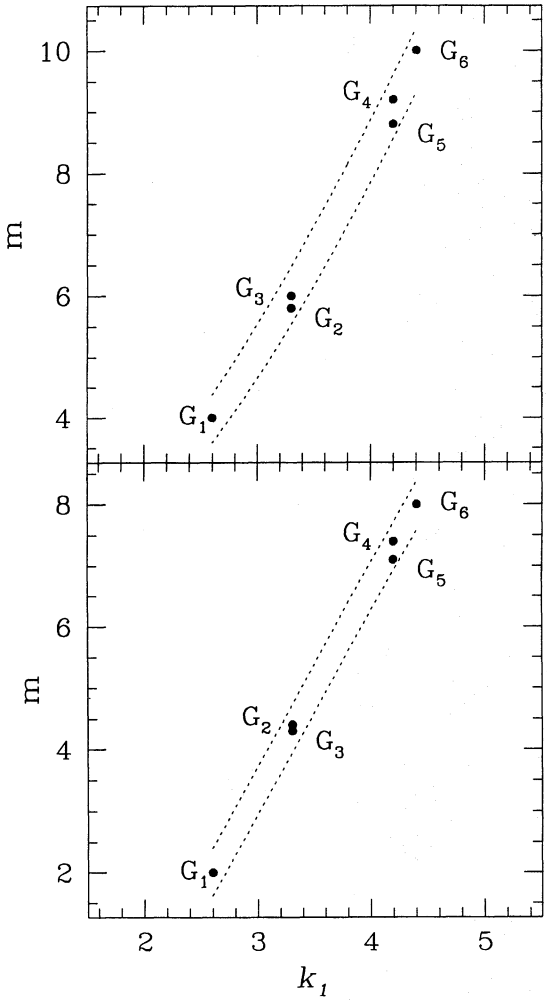

Figure 5. The values of m for the six reference models G_i required to produce the FP tilt in $R^{1/m}$ models, and the band within which m can vary at each location on the k_1-axis in accordance with the observed FP tightness. In the upper panels, the faintest model is characterized by $m=4$; in the lower panel, $m=2$ at the faint end of the FP.

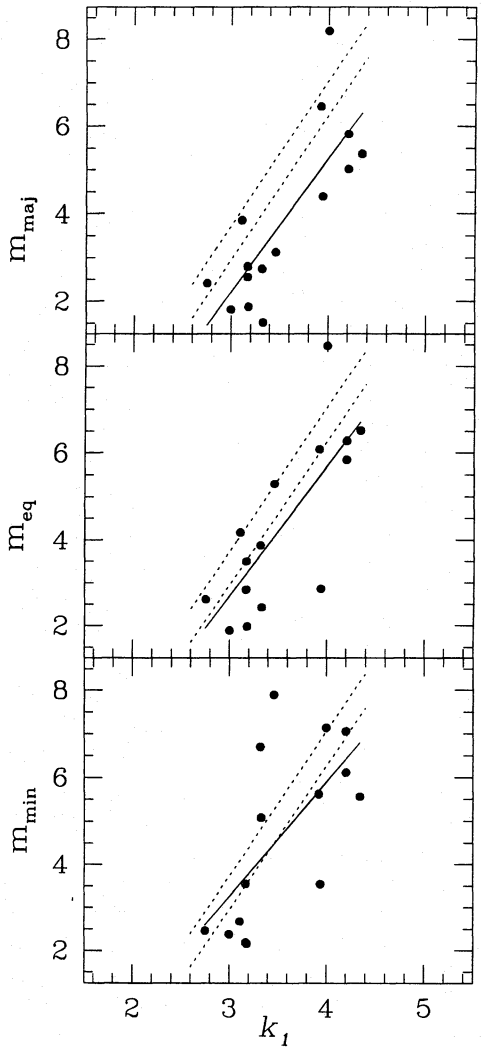

Figure 6. Values of m as fitted by CCD along the major (upper panel), equivalent (middle panel) and minor (lower panel) axis light profile for the Virgo ellipticals in common with BBF. The solid line is the data points best-fitting line; the dotted lines mark the boundary of the permitted variation band of m, in accordance with the observed FP tightness (the same as in Fig. 5, lower panel).

However, as shown in BBF fig. 5, the corresponding decrease in the value of c_2^* is not sufficient to account for the FP tilt, in contrast with our result. However, King models are characterized by a flat core, at variance with high-resolution ground-based and *HST* observations which suggest an increasing density towards the very central regions of elliptical galaxies (Lauer et al. 1992a,b). Therefore we cannot consider our result to be injured by such an argument.

We conclude that further observational studies are required in order to determine whether or not a progression of light profile shapes along the FP really exists among cluster ellipticals.

6 DISCUSSION AND CONCLUSIONS

In this paper we have investigated possible structural or dynamical origins for the observed tilt of the fundamental plane of elliptical galaxies, considering in turn a systematic variation along the FP in the radial orbital anisotropy, in the dark matter content or distribution, and in the shape of the surface brightness profile. In doing so we have varied one such parameter at a time, while keeping the other three constant.

Our exploration indicates that all structural/dynamical solutions to the fundamental plane problem are rather unappealing, although some are more so than others. This comes from the strong *fine tuning* that is required, no matter whether the driving parameter is the anisotropy radius (r_a), the amount of dark matter ($\mathscr{R}$), its distribution relative to the bright matter (β) or the shape of the surface brightness distribution (m).

In addition to this, we have excluded a trend in the anisotropy as a possible cause of the tilt because it leads to physically inconsistent models, and specific arguments also militate against global dark matter content. To produce the tilt, the dark-to-bright matter ratio $\mathscr{R}$ should increase along the FP, from its faint to its bright end. This is just the opposite trend than one expects from galactic wind formation models (e.g., Arimoto & Yoshii 1987), the only ones so far that naturally account for the increase of metallicity (as measured by either broad-band colours or the Mg_2 index) with the depth of the potential well (as approximatively measured by σ_0). Here, the deeper the potential well, the less baryonic material is expelled in a supernova-driven wind, thus leading to lower final value of $\mathscr{R}$. Dissipationless merging models – which do not account for the metallicity–σ_0 correlation – would predict that $\mathscr{R}$ should remain constant after a merging event, or in some cases decrease slightly, as less bound, preferentially dark material may escape from the system during the merging event. In conclusion, we do not see any good reason why the dark matter fraction should systematically increase along the FP, and we actually have hints that it may decrease somewhat. We are therefore inclined to exclude the parameter $\mathscr{R}$ from being responsible for the tilt.

Rather more attractive is, instead, the possibility of a systematic decrease of β along the FP. Qualitatively, a trend of this kind is expected if bright/baryonic matter has dissipated deeper into the potential well of small/faint galaxies compared with into big/bright ones. Actually, towards the faint end of the FP galaxies are characterized by a higher surface brightness and stellar density, and lower effective radii: this suggests that in these galaxies the stellar component is more centrally concentrated relative to dark matter compared to galaxies at the other end of the FP (Guzman, Lucey & Bower 1993). Thus, a systematic variation of β appears more plausible than the previous two alternatives, although the fine tuning problem remains.

Somewhat analogous is the case of a systematic trend in the shape of the stellar distribution, for which there appears to be some observational support (CCD). If the surface brightness profile of ellipticals is well described by a generalized de Vaucouleurs law ($R^{1/m}$ law), then an increase of m by a factor of $\sim$2–4 along the FP is sufficient to produce the tilt. The only embarrassment we see with this solution is, again, the required fine tuning.

There remains the possibility of a *hybrid* origin of the tilt, with more than one effect contributing to tilting the FP, for example, a small progression of anisotropy, DM concentration, and shape (m), coupled with a stellar population effect causing a modest increase of Υ_*. This is perhaps a reasonable solution of the tilt problem, yet a very difficult one to test observationally, given that each effect may individually be buried in the observational noise, and yet the combination of all of them may conjure to produce the observed tilt.

Whatever the solution, the tightness of the distribution of Virgo and Coma ellipticals about the FP is clear evidence for a very standardized and synchronized production of elliptical galaxies, at least those in clusters. Hypothetical formation processes that contain a great deal of stochasticity – such as, e.g., late merging of spiral galaxies – are likely to generate disparate final structures (i.e., r_a, $\mathscr{R}$ and β distributions) and stellar age distributions, hence large dispersions about the FP. Such scenarios are clearly not favoured by the very existence of a tight FP correlation.

This study has also shown that models where both dark and bright components follow a Jaffe density distribution (JJ models) may offer a better description of elliptical galaxies. In general, this applies to models where the DM distribution is similar to the stellar one, albeit less concentrated (see also Dubinski & Carlberg 1991; BSS; Kochanek 1993, 1994). Instead, centrally flat DM distributions frequently give physically or astrophysically unacceptable results, such as velocity dispersion profiles that steeply increase outward, and negative values of their distribution function (Ciotti & Pellegrini 1992). Furthermore, a core radius for the DM haloes is hardly justifiable for dissipationless formation, as the gravitational force is not characterized by any specific scalelength.

ACKNOWLEDGMENTS

We thank Ralf Bender, James Binney, Nicola Caon, George Djorgovski, Mauro D'Orofrio, Silvia Pellegrini and Massimo Stiavelli for useful discussions. This work was supported in part by the Italian Ministry of Research (MURST), and in part by the Consiglio Nazionale delle Ricerche (CNR).

REFERENCES

Arimoto N., Yoshii Y., 1987, A&A, 173, 23
Bender R., Burstein D., Faber S. M., 1992, ApJ, 399, 462 (BBF)

Bertin G., Saglia R. P., Stiavelli M., 1992, ApJ, 384, 423 (BSS)
Bertin G. et al., 1994, A&A, 292, 381
Binney J., 1980, MNRAS, 190, 873
Binney J., Tremaine S., 1987, Galactic Dynamics. Princeton Univ. Press, Princeton, NJ (BT)
Caon N., Capaccioli M., D'Onofrio M., 1993, MNRAS, 265, 1013 (CCD)
Carollo C. M., Danziger I. J., 1994a, MNRAS, 270, 523
Carollo C. M., Danziger I. J., 1994b, MNRAS, 270, 743
Carollo C. M., de Zeeuw P. T., van der Marel R. P., Danziger I. J., Qian E. E., 1995, ApJ, 441, L25
Ciotti L., 1991, A&A, 249, 99
Ciotti L., Pellegrini S., 1992, MNRAS, 255, 561
Davies R. L., Efstathiou G., Fall S. M., Illingworth G., Schechter P. L., 1983, ApJ, 266, 41
de Vaucouleurs G., 1948, Ann. d'Astrophys., 11, 247
Djorgovski S. G., 1995, ApJ, 438, L29
Djorgovski S. G., Davis M., 1987, ApJ, 313, 59
Djorgovski S. G., Santiago B. X., 1993, in Danziger I. J., Zeilinger W. W., Kjär K., eds, Structure, Dynamics and Chemical Evolution of Elliptical Galaxies. ESO, Garching, p. 59
Dressler A., Lynden-Bell D., Burstein D., Davies R. L., Faber S. M., Terlevich R. J., Wegner G., 1987, ApJ, 313, 42 (D87)
Dubinski J., Carlberg G., 1991, ApJ, 378, 496
Guzman R., Lucey J. R., Bower R. G., 1993, MNRAS, 265, 731
Hernquist L., 1990, ApJ, 356, 359
Hjorth J., Madsen J., 1995, ApJ, 445, 55
Jaffe W., 1983, MNRAS, 202, 995
King I., 1996, AJ, 71, 64
Kochanek C. S., ApJ, 1993, 419, 12
Kochanek C. S., ApJ, 1994, 436, 56
Lauer T. R. et al., 1992a, AJ, 103, 703
Lauer T. R. et al., 1992b, AJ, 104, 552
Makino J., Akiyama K., Sugimoto D., 1990, PASJ, 42, 205
Merritt D., 1985a, AJ, 90, 1027
Merritt D., 1985b, MNRAS, 214, 25P
Osipkov L. P., 1979, Pis'ma Astron. Zh., 5, 77
Plummer H. C., 1911, MNRAS, 71, 460
Renzini A., 1995, in Gilmore G., van der Kruit P., eds, Stellar Populations. Kluwer, Dordrecht, p. 325
Renzini A., Ciotti L., 1993, ApJ, 416, L4 (RC)
Saglia R. P., Bertin G., Stiavelli M., 1992, ApJ, 384, 433 (SBS)
Sersic J. L., 1968, Atlas de galaxias australes. Observatorio Astronomico, Cordoba
van Albada T. S., 1982, MNRAS, 201, 939

APPENDIX A: VELOCITY DISPERSION PROFILES FOR HH, HP AND JJ MODELS

With the assumed radial trend for the velocity dispersion tensor, the solution of the Jeans equation can be written in integral form, as shown by Binney (1980). Moreover, for our two-component models the solutions can be obtained in closed form, and we give the resulting radial velocity dispersions. The tangential component can be successively obtained by using equation (12). In order to avoid a cumbersome notation, we define the dimensionless variables $s \equiv r/r_*$ and $s_a \equiv r_a/r_*$. It is straightforward to show that the general velocity dispersion for our models looks like

$$\rho_*(r)\,\sigma_r^2(r) = \frac{GM_*^2}{2\pi r_*^4}\,\frac{(A_{**}+s_a^2 I_{**}) + \mathscr{R}\,(A_{*D}+s_a^2 I_{*D})}{s^2+s_a^2}, \tag{A1}$$

where the functions A_{**} and I_{**} depend on the stellar density distribution only, and I_{*D} and A_{*D} are the interaction terms due to the DM gravitational field. Note that when the velocity dispersion is completely isotropic (i.e. $s_a \to \infty$) only the I functions remain; on the contrary, in the formal case of completely radial orbits ($s_a = 0$), the velocity dispersion is described by the A functions. For the Hernquist and Jaffe stellar profiles, the two components due to the pure stellar distribution are respectively given by

$$A_{**} = \frac{4s+1}{12(1+s)^4}, \tag{A2}$$

$$I_{**} = -\frac{12s^3+42s^2+52s+25}{12(1+s)^4} - \ln\frac{s}{1+s}, \tag{A3}$$

and

$$A_{**} = -\frac{1}{2}\left[\frac{2s+3}{2(1+s)^2} + \ln\frac{s}{1+s}\right], \tag{A4}$$

$$I_{**} = -\frac{1}{2}\left[\frac{(6s^2+6s-1)(2s+1)}{2s^2(1+s)^2} + 6\ln\frac{s}{1+s}\right]. \tag{A5}$$

We now give the interaction terms for the various distributions. Starting with the HH models, we have

$$A_{*D} = -\frac{1}{2(\beta-1)^2(1+s)^2} + \frac{\beta+1}{(\beta-1)^3(1+s)} + \frac{\beta}{(\beta-1)^3(\beta+s)} + \frac{2\beta+1}{(\beta-1)^4}\ln\frac{1+s}{\beta+s}, \tag{A6}$$

$$I_{*\mathrm{D}}=-\frac{1}{2(\beta-1)^2(1+s)^2}+\frac{1}{\beta(\beta-1)^3(\beta+s)}-\frac{\beta-3}{(\beta-1)^3(1+s)}-\frac{\ln s}{\beta^2}+\frac{(\beta^2-4\beta+6)\ln(1+s)}{(\beta-1)^4}-\frac{(4\beta-1)\ln(\beta+s)}{\beta^2(\beta-1)^4}. \tag{A7}$$

For HP models the functions are more complicated, owing to the different qualitative behaviour of the density distributions. After lengthy calculations, we find

$$A_{*\mathrm{D}}=\frac{5(2\beta^2-1)}{2(1+\beta^2)^3}-\frac{s^3(10\beta^2-5)+s^2(2\beta^4+9\beta^2-8)+s(8\beta^4-9\beta^2-2)+(5\beta^4-10\beta^2)}{2(1+\beta^2)^3(1+s)^2\sqrt{\beta^2+s^2}}$$

$$-\frac{2\beta^4-11\beta^2+2}{2(1+\beta^2)^{7/2}}\ln\frac{(1+s)(\sqrt{1+\beta^2}-1)}{\sqrt{(1+\beta^2)(\beta^2+s^2)}+\beta^2-s} \tag{A8}$$

and

$$I_{*\mathrm{D}}=\frac{(2-13\beta^2)}{2\beta^2(1+\beta^2)^3}+\frac{s^3(13\beta^2-2)+s^2(3\beta^4+14\beta^2-4)+s(11\beta^4-6\beta^2-2)+(\beta^6+10\beta^4-6\beta^2)}{2(1+s)^2\beta^2(1+\beta^2)^3\sqrt{\beta^2+s^2}}$$

$$+\frac{3(\beta^2-4)}{2(1+\beta^2)^{7/2}}\ln\frac{(1+s)(\sqrt{1+\beta^2}-1)}{\sqrt{(1+\beta^2)(\beta^2+s^2)}+\beta^2-s}. \tag{A9}$$

Finally, for JJ models, we have

$$A_{*\mathrm{D}}=-\frac{1}{2}\left[\frac{1}{(\beta-1)(s+1)}+\frac{\ln s}{\beta}-\frac{(\beta-2)\ln(1+s)}{(\beta-1)^2}-\frac{\ln(\beta+s)}{\beta(\beta-1)^2}\right], \tag{A10}$$

$$I_{*\mathrm{D}}=-\frac{1}{2}\left[\frac{2s^2(3\beta^2-\beta-1)+s(3\beta^2-\beta-2)-\beta(\beta-1)}{2s^2\beta^2(\beta-1)(1+s)}-\frac{(3\beta^2+2\beta+1)\ln s}{\beta^3}+\frac{(3\beta-4)\ln(1+s)}{(\beta-1)^2}+\frac{\ln(\beta+s)}{\beta^3(\beta-1)^2}\right]. \tag{A11}$$

Note that the singularity for $\beta=1$ in $A_{*\mathrm{D}}$ and $I_{*\mathrm{D}}$ for HH and JJ models can be eliminated, for in the limit $\beta\to1$ these expressions coincide with the corresponding A_{**} and I_{**}.